International Journal of Pharmaceutics 635 (2023) 122691

Contents lists available at ScienceDirect

International Journal of Pharmaceutics

journal homepage: www.elsevier.com/locate/ijpharm

Development and implementation of a pneumatic micro-feeder for poorly-flowing solid pharmaceutical materials

P. Hou [a,b], M.O. Besenhard [c], G. Halbert [a,b], M. Naftaly [d], D. Markl [a,b,*]

[a] Strathclyde Institute of Pharmacy and Biomedical Sciences, University of Strathclyde, Glasgow G1 1XQ, UK
[b] Centre for Continuous Manufacturing and Advanced Crystallisation (CMAC), University of Strathclyde, Glasgow G1 1RD, UK
[c] Department of Chemical Engineering, University College London, London WC1E 7JE, UK
[d] National Physical Laboratory, Teddington TW11 0LW, UK

ARTICLE INFO

Keywords:
Powder feeding
Micro-feeding
Continuous feeding
High accuracy
Pneumatic transferring

ABSTRACT

Consistent powder micro-feeding (<100 g/h) is a significant challenge in manufacturing solid oral dosage forms. The low dose feeding can well control the content consistency of the dosage forms, which improves drug efficiency and reduces manufacturing waste. Current commercial micro-feeders are limited in their ability to feed < 20 g/h of cohesive (i.e. powders of poor flowability) active pharmaceutical ingredients (API) and excipients (e.g. lubricants) with low fluctuation. To breach this gap, this study presents an advanced micro-feeder design capable of feeding a range of pharmaceutical-grade powders consistently at flow rates as low as 0.7 g/h with <20 % flow rate variation. This was possible due to a novel powder conveying concept utilising particle re-entrainment to minimise flow rate variations. This work details the design of this pneumatic micro-feeder and its excellent micro-feeding performance even for cohesive powders. The experimental studies investigated the influence of the process parameters (air pressure and air flow rate) and equipment configurations (insert size and plug position) on the feeding performance of different pharmaceutical-relevant powders, i.e., microcrystalline cellulose (MCC), croscarmellose sodium (CCS), crospovidone (XPVP) and paracetamol (APAP). It was shown that the system is capable of delivering consistent powder flow rates with good repeatability and stability.

1. Introduction

Continuous and consistent powder feeding is feeding powder in the range of grams per hour with low flow rate deviation. It is required in various industries, especially in the pharmaceutical sector. With the pharmaceutical industry moving more toward continuous manufacturing of drug products (Blackshields and Crean, 2018), consistent, accurate and continuous feeding of the individual components of the formulation are crucial to meet the required quality of the final product (Nagy et al., 2020). Inconsistent feeding can degrade content uniformity and performance of the final product and hence can lead to out-of-specification products (Engisch and Muzzio, 2014). Therefore, continuous feeding of small quantities of powder remains a challenge, especially during the feeding of cohesive or electrostatic powders in which the particles tend to stick together or adhere on a contact surface, i.e. hopper wall or screw.

Growing markets such as small-scale clinical trial material (CTM), high-potency API (HPAPI) and personalised medicine manufacturing are in need of feeding small quantities of materials with high accuracy. These processes include the consistent feeding of low ratios of active pharmaceutical ingredients (APIs), lubricants and disintegrants for a given formulation in continuous drug manufacturing processes (Burcham et al., 2018), seeding in the crystallisation process (Ramachandran et al., 2017), manufacturing of low-dose products of high-potency active pharmaceutical ingredients (HPAPI) (Bostijn et al., 2019; Engisch and Muzzio, 2014), production of personalised medicines (Raijada et al., 2021) and direct dosing API to capsules (Stranzinger, 2018).

Consistent micro-feeding also plays an essential role in the application of 3D-printed medicine (Quodbach et al., 2021). Loss-in-weight (LIW) feeders are widely used in material feeding to 3D printers, and are utilised to minimise feed rate fluctuations. However, LIW feeders still cannot satisfy the consistency required for 3D-printed drugs or personalised medicines, especially when feeding cohesive or sticky materials (Quodbach et al., 2021). The 3D printing of drugs or personalised medicines highly depends on consistent and continuous feeding (Jamróz et al., 2018; Oladeji et al., 2022; Jassim-Jaboori and Oyewumi,

* Corresponding author at: Strathclyde Institute of Pharmacy & Biomedical Sciences, University of Strathclyde, Glasgow, UK.
E-mail address: daniel.markl@strath.ac.uk (D. Markl).

https://doi.org/10.1016/j.ijpharm.2023.122691
Received 21 November 2022; Received in revised form 31 January 2023; Accepted 2 February 2023
Available online 8 February 2023

Table 1
General variables that influence the powder feeding performance.

Material properties	Process parameters	Environmental conditions
Particle size and shape	Pressure	Consolidation
Surface area	Temperature	Aeration
Bulk density	Vibration	Humidity level
True density	Hopper design	The extent of shear/ strain
Cohesion	Refill	Equipment surface properties
Adhesion	Connections	Excessive plant vibration
Elasticity	Controls and weight measurement	
Plasticity	Equipment construction materials	
Porosity		
Electrostatic charge	Other process parameters depending on the operating principle (vibratory, screw etc.)"	
Hardness/ Friability		

2015). A failed formulation can lead to the weak breaking strength of the tablets or poor drug release profiles to be delivered to specific parts of the body.

Consistent powder feeding is highly dependent on powder properties, such as particle size distribution, cohesion force between particles and adhesion force between particles to the equipment contact surface. In reality, new APIs and many excipient powders are classified as cohesive or poorly flowing materials. Cohesive materials are susceptible to aggregate, reduce powder's movement and stick to the equipment, eventually causing high variations in the flow rate. It is a great challenge to develop a powder feeder that can continuously and reproducibly feed powder with high consistency regardless of its powder properties.

In a micro-feeder design, the variables influencing powder flow rate accuracy can be categorised into three groups: material properties, process parameters and environmental conditions. The powder flow rate consistency is typically a non-linear function of the different variables. Table 1 lists and groups the variables that influence feeder performance that should be considered during a powder feeder design. Out of these variables, however, only the process parameters can be controlled in the micro-feeder design.

The current powder micro-feeder concepts such as screw feeder (Barati Dalenjan et al., 2015; Engisch and Muzzio, 2015), vibrating feeder (Besenhard et al., 2016, 2015; Wang et al., 2018b), pulse inertia force feeder (Wang et al., 2018a) and powder pump feeder (Besenhard et al., 2017; Fathollahi et al., 2021, 2020) were developed by adapting different process parameters to overcome various powder properties in order to achieve consistent feeding. Table 2 lists the current studies of micro-feeders and their concepts and performance. For example, vibratory feeders use vibrations to overcome poor powder movement caused by cohesion issues; the pulse inertia force feeder uses the pulse inertia force to overcome interparticle cohesive forces in small capillaries to drive powder movement. The powder pump uses a plunger to push powder upward to eliminate the powder movement issue. It then uses packing the powder in a cartridge to minimise the varying bulk density caused by the wall friction or compression during powder transfer. Each feeder, however, has its limitations. For example, the vibratory feeder has severe segregation issues and requires sharp particle size distributions for consistent micro-feeding. The vibrating frequency and vibrating chute design are also determine the feeder performance. The performance of the screw feeder is affected by the particle size and compression status. Others, like the hopper size, shape, and screw types, can influence the performance of a feeder. Due to friction, the capillaries in the pulse inertia force feeder are easily blocked by powder. Although the powder pump can feed at low-dose rates with different particle sizes and flow properties, it still shows its limitations: 1. Pre-conditioning is required before feeding; 2. Using a scraper causes additional compression as the plunger keeps moving up while the scraper may temporarily close the cartridge outlet; 3. The wall friction causes the packing density variation while the plunger pushes upward. It causes high fluctuations and influences the powder flow rate.

Powder entrainment in pneumatic conveying has been studied in the last 30 years (Annamalai et al., 1992; Hartman et al., 2006; Matsusaka and Masuda, 1996; Suri and Horio, 2009). This powder entrainment principle is utilised in the pneumatic micro-feeder. The papers indicate that the moment forces: adhesion force, drag force and gravity are required to entrain a particle. In this study, the sum of these forces is called "entrainment force". This force is seen as the minimum force to pick up a particle from stationary status. Based on this principle, when a constant force (fixed air pressure and flow rate) is continuously supplied to the system, it will only entrain a certain amount of particles. Slight adjustments in entrainment force overcome time-to-time variations in cohesion and particle size distribution.

Table 2
Previous studies of powder micro-feeders.

Year	Author	Materials	Feed rates (g/h)	Variation	D_{50} (μm)	Hausner ratio (-)	Concept
1999	Tang et al.	Geldart A particles including coal and coal-derived char particles	0.6–31.8	<5%	20–250	NA	Sweeping the particles upward into a concentric tube which also serves as the piston support.
2012	Chen et al	Lactose Powder	3.6–36	<3%	66–206	1.12–1.23	Vibrating capillary
2014	Zainuddin *et al.*; Horio et al.	Microcrystalline cellulose	86.4–306	3–5 %	50–170	1.26–1.79	Vibration shear tube method
2015	Dalenjan et al.	Zinc oxide	72–630	2–14 %	<10	7.00	Screw-brush feeding system
2016	Besenhard *et al.*	Inhalac 230 Respitose SV003	3.6 – 7.2	4.6–12 %	90–160	1.21–1.24	Vibratory sieve chute system
2017	Besenhard *et al.*	α-lactose monohydrate powders	1–100	4–20 %	71.0 – 204.4	1.18–1.84	Powder pump (cylinder-piston feeder)
2018	Wang *et al.*	Respitose SV003 Granulac 230	1.44–1.8	<12 %	71–77.5	1.27–1.51	Micro-Dosing of fine cohesive powders actuated by a pulse inertia force
2020	Fathollahi et al.	CapsuLac 60 GranuLac 200 Di-calcium phosphate Croscarmellose sodium Silicon dioxide API A SDI B	1–20	10–20 %	20.2–243.7	1.10–1.79	Powder pump (cylinder-piston feeder)

*Hausner ratio is a ratio of the tapped density (ρ_t) to bulk density (ρ_b) and is commonly used to quantify a powder's flowability. The flowability is an indicator to identify the powder flow behaviour. The higher value Hausner ratio is, the poorer flow material behaves (McGlinchey, 2009; Schulze et al., 2008). The powder flow refers to the movement ability of powder in an equipment. The indication of flowability can be found in Table S1 in the supporting information.

Table 3
Material properties of the experimental materials.

Powders	D_{10} (μm)	D_{50} (μm)	D_{90} (μm)	S_{50} (-)	True Density (g/cm^3)	Bulk Density (g/cm^3)	Tapped Density (g/cm^3)	Hausner ratio (-)	Flowability
Microcrystalline cellulose (MCC)	56.6 ± 4.0	139.4 ± 11.7	238.9 ± 6.2	0.63 ± 0.007	1.5423 ± 0.001	0.314 ± 0.036	0.447 ± 0.036	1.43 ± 0.061	Cohesive
Croscarmellose Sodium (CCS)	29.9 ± 0.1	50.0 ± 0.1	74.2 ± 0.1	0.72 ± 0.003	1.5367 ± 0.010	0.529 ± 0.001	0.715 ± 0.001	1.35 ± 0.000	Cohesive
Crospovidone (XPVP)	30.1 ± 0.1	103.4 ± 0.3	244.0 ± 1.0	0.73 ± 0.001	1.1830 ± 0.003	0.334 ± 0.001	0.451 ± 0.001	1.35 ± 0.000	Cohesive
Paracetamol (APAP)	23.6 ± 0.1	67.9 ± 0.4	178.1 ± 3.8	0.63 ± 0.003	1.2906 ± 0.002	0.310 ± 0.003	0.495 ± 0.005	1.60 ± 0.029	Non-flow

The shown values are the mean ± standard deviation of all measurements in triplicate.
D_{10},D_{50} and D_{90} are respectively the mean particle size below which 10 %, 50 % or 90 % of all particles are contained.
Volume mean diameter (*VMD*): Average particle size diameter per volume of the particles
S_{50} is the sphericity below 50 % of all particles contained.

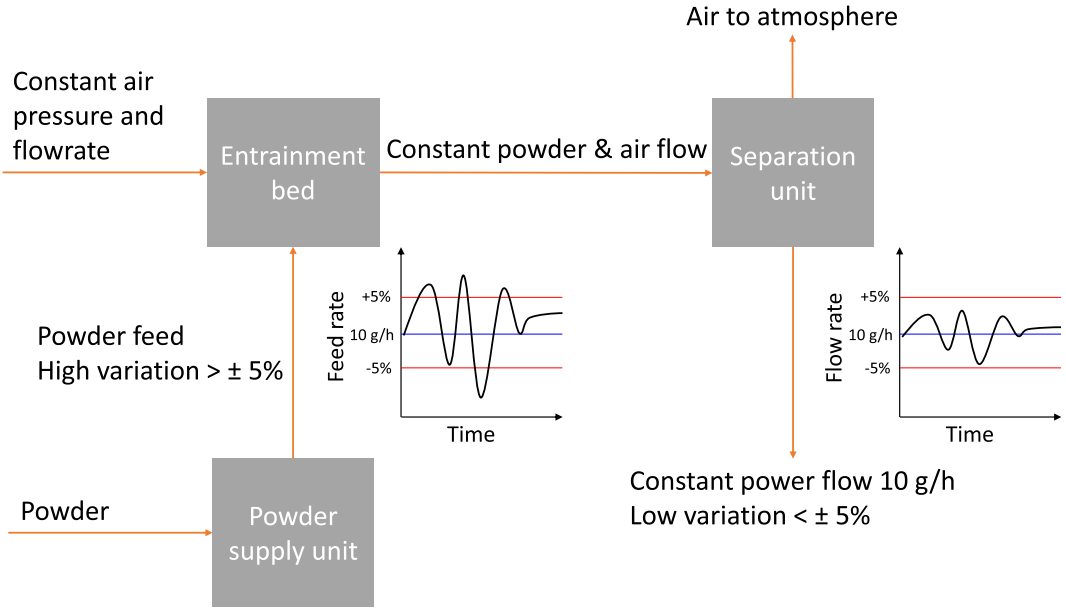

Fig. 1. A process flow diagram for the proposed micro-feeder's conceptual design.

This study presents a pneumatic micro-feeder that enables highly consistent feeding. This system is based on the effect of powder entrainment to control the powder flow rate. The air entrainment concept is deployed to minimise agglomeration as the air flow minimises particle–particle and particle–wall contacts (Francis et al., 2010; Kousaka et al., 1980; Theerachaisupakij et al., 2003). This study describes the detailed principle and equipment setup (section 2.2). It assesses the impact of process parameters and equipment configurations (section 3.3) on feeding performance using four pharmaceutical-grade powders (section 3.4) to cover various powder properties.

2. Materials and method

2.1. Materials

Four powders with a wide range of properties were used to assess the performance of the feeder design: microcrystalline cellulose (MCC) (VIVAPUR 112 from JRS pharma, Germany), croscarmellose sodium (CCS) (JRS pharma, Germany), crospovidone (XPVP) (Kollidon® CL, BASF), and an active pharmaceutical ingredient, paracetamol (APAP) (Ph Eur Powder from Mallinckrodt Pharmaceuticals, Ireland). The selected MCC is a common material used as a filler in typical tablet formulations. It is selected to understand this system's powder behaviour and optimise the system. Croscarmellose sodium and crospovidone are common disintegrants. Both materials have similar flowability but different particle size, facilitating the particle size assessment of the feeder performance. Paracetamol is a common API. It represents a poor flowability material and typical powder properties of APIs in this study. Table 3 summarises the powder properties of the experimental materials. The methods used for powder characterisation, together with further results can be found in the supporting information section 1.

2.2. Pneumatic micro-feeder

The pneumatic micro-feeder uses a powder supply unit to feed powder into the system and control the mean powder flow rate. A stable air flow is then to entrain and convey the particles and, importantly, minimise powder flow rate variations. Fig. 1 shows the flow diagram of this pneumatic micro feeder prototype.

Fig. 2a depicts the pneumatic micro-feeder design with a validation balance comprising an air supply line, an entrainment bed, a powder supply unit and a cyclone separator. The pneumatic micro-feeder is designed in modules, where each component can be independently manufactured, modified and replaced. The modular design facilitates to

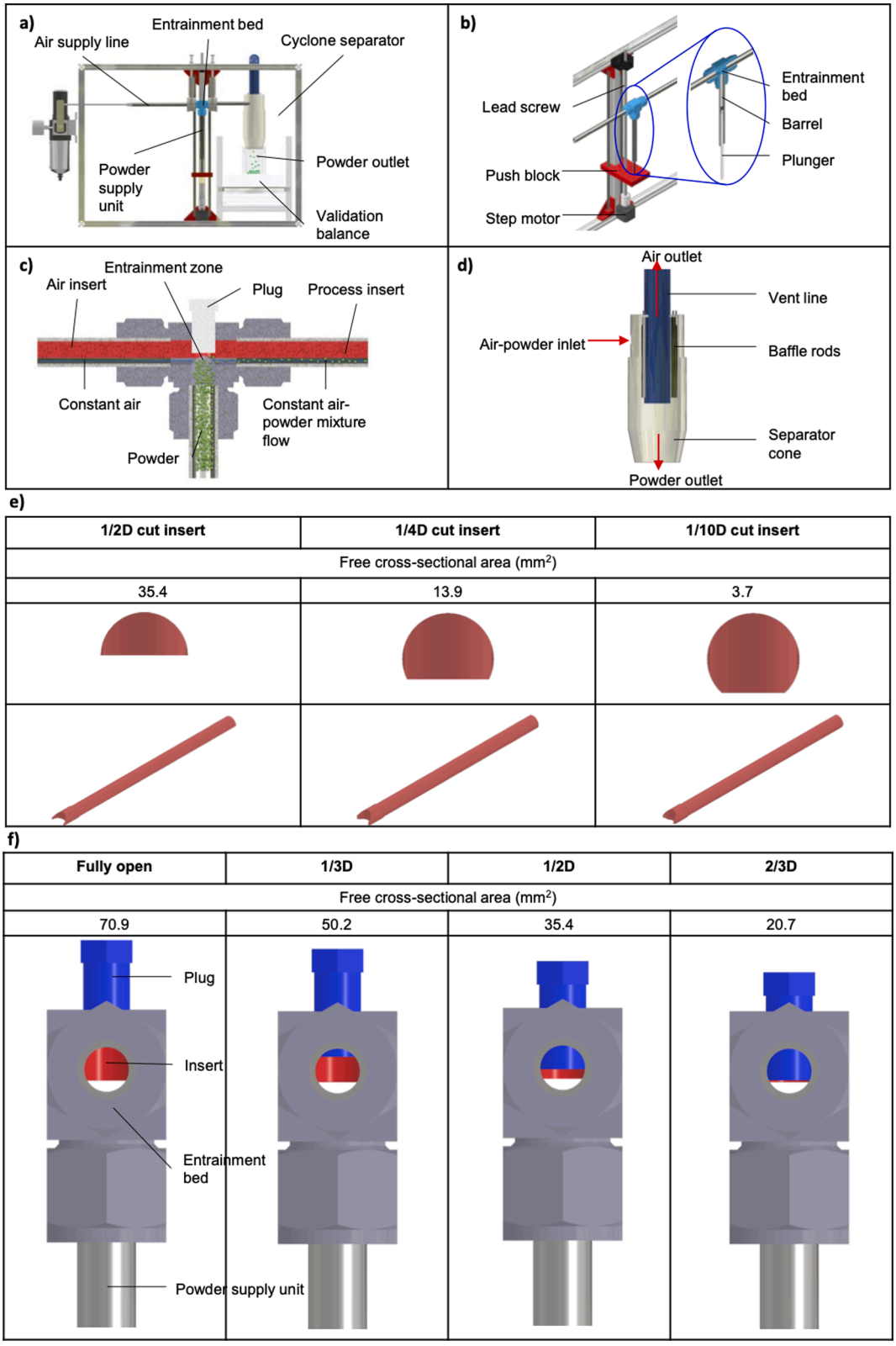

Fig. 2. Prototype of the micro-feeder system with (a) overview, (b) powder pump, (c) entrainment bed half-section view, (d) cyclone separator, (e) air supply line and process lines insert types (side view and top-front-right view), (f) plug position to regulate air velocity in the chamber (side view).

analyse and identify the critical components that affect the system's performance; each component can then be optimised individually. A photo of the pneumatic micro-feeder is shown in Figure S1 in the supporting information.

The air supply line provides constant air pressure and flow rate to the system. It comprises a pressure regulator (Norgren-E74H-4GK-QD1-NFG-QPB, Norgren) and a variable area air flowmeter (WZ-32460–48, Masterflex, Cole-Parmar). The powder supply unit is a powder pump (Fig. 2b) adapted from Besenhard et al. (2017). Its purpose is the supply of powder material into the entrainment bed and controls the mean

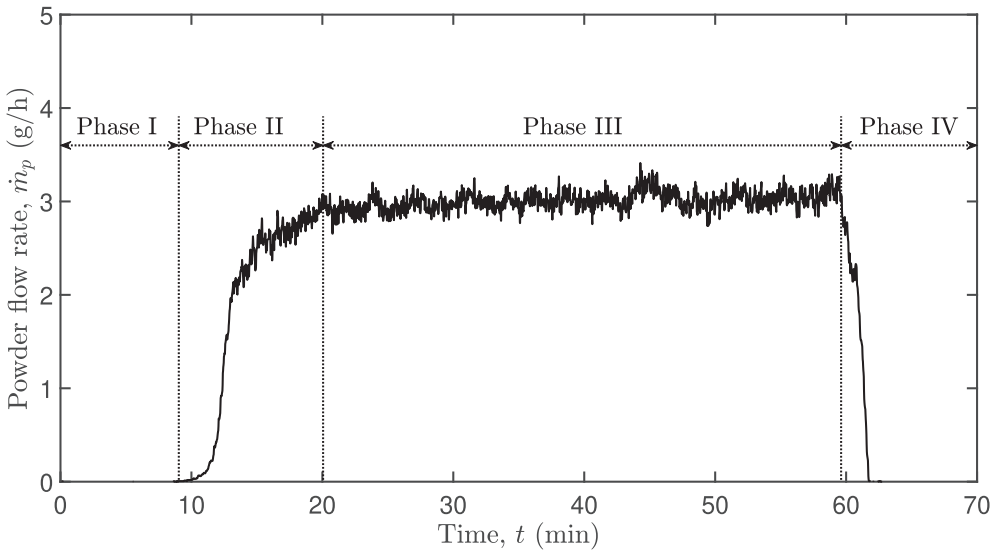

Fig. 3. MCC powder feeding process at a feed rate of 3 g/h. Process parameters: piston speed of 2 mm/min; air pressure of 25 kPa; air flow rate of 4 l/min.

powder flow rate. The use of the powder pump provides a relatively simple feeding mechanism compared to other feeders that involve a complex mechanical design such as a vibration-generation system. The powder pump length is 120 mm in this study. The effect of piston speed is discussed in section 3.3.1.

The entrainment bed (Fig. 2c),where the powder is entrained, produces the air-powder mixture. The entrainment bed is an adapted 1/2 in. PFA union tee with a tube fitting (PFA-820–3, Swagelok). In this prototype, inserts (Fig. 2e) and plugs (Fig. 2f) are applied to narrow the chamber of the entrainment bed and the process and air lines. Fig. 2e depicts the air supply line insert types to regulate the air velocity to the entrainment bed, and the process lines insert types to maintain the powder-air flow velocity. The inserts are labelled according to their free cross-section area, e.g. 1/4D corresponds to a circular segment with a height equal to 1/4 of the tube diameter. Fig. 2f depicts plug positions to regulate air velocity in the chamber. The plug positions are labelled according to position in the chamber, e.g. 1/3D corresponds to a circular segment with a height equal to 2/3 of the tube diameter. The size of the process line insert is 1/4D cut as shown in Fig. 2e. Therefore, the plug and the insert are used to 1) maintain the desired air velocity and pressure drop with low air supply; 2) increase the entrainment rate and efficiency; 3) enable the system to handle a wider range of material properties; 4) minimise the accumulation built up in the chamber; 5) reduce the air consumption and workload to the separator. The effects of insert size and plug position are discussed in sections 3.3.2 and 3.3.3.

A cyclone separator is a well-developed technique with no moving parts and a small number of control parameters. It is used to separate the powder-air stream (Fig. 2d). Eight vertical baffle rods are installed inside the separator to improve the separation efficiency through impinging particles on the vertical baffle rods. In addition, the separator can be equipped with a vibration motor (Seeed Studio 105,020,003 Grove-Vibration Motor) to minimise the powder fouling formed on the separator wall due to the adhesive forces. To measure the powder flow rate, a lab-scale balance (60|120 g, ±0.01|±0.1 mg, Sartorius Quintix 125D-1S, Germany) is mounted beneath the cyclone separator outlet. The balance was calibrated before the daily experiments followed by an annual calibration and maintenance.

2.3. Methods

Four pharmaceutical-grade powders (Table 3) at three piston speeds were studied to assess the performance of the pneumatic micro-feeder. The appropriate insert size and plug positions were selected to suit different powder properties as shown in the Fig. 2e and f respectively. The piston speed is the displacement speed at which the powder is pushed upwards. This speed was controlled by a stepper motor which had been calibrated prior to the experiments, i.e. 1 rpm of motor speed equals 1 mm/min of piston speed in the current setup. The air pressure and air flow rate were fixed for each experiment. This is given for each experiment in the caption of each figure. In addition, there was no preconditioning of the powder needed for the application of the pneumatic micro-feeder. The accumulated powder weight (g) was recorded every second. Section 3.2 examines each variable's effects on the stability and repeatability of the system.

Several values are calculated to assess the performance of the micro-feeder:

Powder flow rate ($\dot{m}_p$) is the average powder flow rate calculated when the powder flow rate plateaued (Phase III as shown in Fig. 3), i.e. from 20 min to the end of phase III (59 min) at an air flow rate of 4 l/min with the piston speed of 2 mm/min for MCC (Fig. 3).

$$\dot{m}_p = \frac{1}{n}\sum_{j=1}^{n}(m_{t_{j+1}} - m_{t_j})/(t_{j+1} - t_j), \tag{1}$$

where m_j and m_{j+1} are the accumulated powder weights at measurement times t_j and t_{j+1}. j is the measurement index (1 s). n is the number of samples in phase III, e.g. n = 2340 (from 20 min to 59 min) in Fig. 3 case.

Average powder flow rate ($\overline{\dot{m}_p}$) is the mean of a powder flow rate of three repeated experiments:

$$\overline{\dot{m}_p} = \frac{1}{3}\sum_{i=1}^{3}\dot{m}_{p,i}. \tag{2}$$

with i as the number of experiments.

Standard deviation (σ) represents a measure of differences in powder flow rates from the average powder flow rate:

$$\sigma = \sqrt{\frac{1}{n-1}\sum_{j=1}^{n}\left|\dot{m}_j - \dot{m}_p\right|^2}, \tag{3}$$

where $\dot{m}_j$ represents an individual powder flow rate after the flow rate is stabilised (Phase III).

Relative standard deviation (*RSD*) is obtained by dividing the standard deviation by the average powder flow rate. In this study, this value indicates the variation of the powder feed rate from the mean powder flow rate. The high value indicates a higher variation and

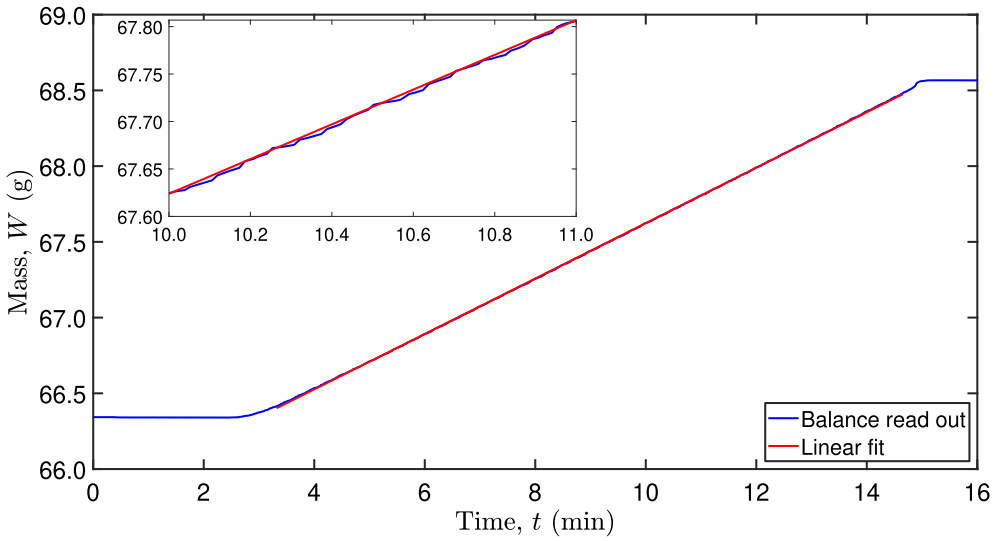

Fig. 4. An example of MCC recorded powder weight at 8 mm/min of piston speed with a linear line fit (red line). The enlarged view depicts a close view from 10 min to 11 min which demonstrates the acutal dispensed powder weight was close to the linear regression line. It implies a consistent powder feeding. (For interpretation of the references to colour in this figure legend, the reader is referred to the web version of this article.)

indicates poorer accuracy of powder feeding:

$$RSD = \sigma/\dot{m}_p \hat{A}\cdot 100\% \tag{4}$$

Average relative standard deviation ($\overline{RSD}$) is the mean of relative standard deviations of three repeat experiments:

$$\overline{RSD} = \frac{1}{3}\sum_{i=1}^{3} RSD_i. \tag{5}$$

Repeatability (r) is the standard deviation of powder flow rates of three repeat experiments divided by the average powder flow rate:

$$r = \sqrt{\frac{1}{2}\sum_{i=1}^{3}|\dot{m}_{p,i} - \overline{\dot{m}_p}|^2/\overline{\dot{m}_p}}\hat{A}\cdot 100\% \tag{6}$$

Stability (s) is the standard deviation of three relative standard deviations from three repeat experiments. It is defined as

$$s = \sqrt{\frac{1}{2}\sum_{i=1}^{3}|RSD_i - \overline{RSD}|^2}\hat{A}\cdot 100\%. \tag{7}$$

3. Results and discussions

3.1. Micro-feeder performance statistics

For the performance analysis, the powder weight is recorded at 1 Hz via a data logger. The powder flow rate is expressed as $\dot{m}_p(t) = \Delta m/\Delta t$, where Δm is the powder mass accumulated within a certain time window Δt. Fig. 4 shows an example of raw data of MCC feeding, demonstrating that the raw data closely follows a linear trend.

Due to the measurements being recorded in an 'unstable' condition, this lab-scale balance used in this study provides an average value of two or three mass measurements, i.e. a data point recorded from the balance at a rate of 1 s interval is an average of two or three individual mass measurements in a second internally in the balance. For continuous

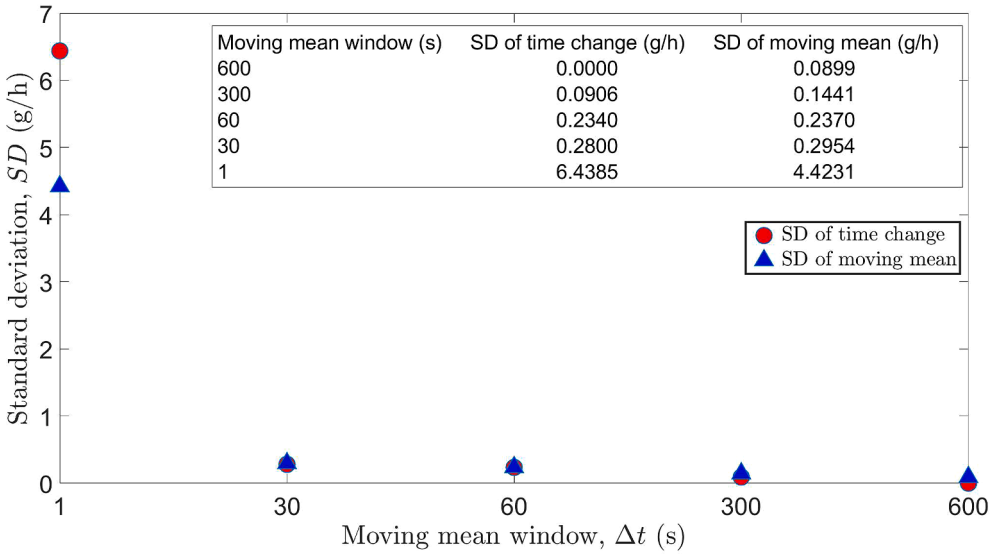

Moving mean window (s)	SD of time change (g/h)	SD of moving mean (g/h)
600	0.0000	0.0899
300	0.0906	0.1441
60	0.2340	0.2370
30	0.2800	0.2954
1	6.4385	4.4231

Fig. 5. Standard deviations as a function of applying time changes and moving mean windows for a powder feeding at 11 g/h.

Table 4
A summary of phases I, II and III at various piston speeds for the different materials.

Material	Piston speed, S (mm/min)	Air pressure, P (kPa)	Air flow rate, Q (l/min)	Air mass flow rate, $\dot{m}_{air}$ (g/h)	Average compression phase, $t_{Phase\ I}$ (min)	Compression length, $L_{c,actual}$ (mm)	Compressibility, C (%)	Acceleration phase, $t_{Phase\ II}$ (min)	Stable feeding phase, $t_{Phase\ III}$ (min)
MCC	8	25	9	157.7	2.1 ± 0.0	17.0 ± 0.3	6.7 ± 0.2	1.9 ± 0.2	10.9 ± 0.2
	7	25	8	140.2	2.6 ± 0.0	17.9 ± 0.3	7.4 ± 0.2	1.8 ± 0.1	12.8 ± 0.2
	4	25	5	87.6	4.4 ± 0.1	17.4 ± 0.4	7.0 ± 0.4	5.2 ± 0.3	20.5 ± 0.2
	2	25	4	70.1	8.7 ± 0.5	17.5 ± 1.0	7.1 ± 0.8	10.8 ± 1.6	40.5 ± 1.1
	1	25	3	52.6	21.0 ± 2.4	21.0 ± 2.4	10.0 ± 2.0	12.8 ± 1.5	86.3 ± 2.8
APAP	7	50	10	350.5	5.6 ± 1.1	39.0 ± 7.8	25.0 ± 6.5	5.1 ± 1.8	6.5 ± 0.7
	4	30	9	189.3	8.9 ± 0.2	35.4 ± 0.6	22.0 ± 0.5	7.1 ± 1.2	14.1 ± 1.2
	2	25	9	157.7	18.3 ± 2.8	36.6 ± 5.6	23.0 ± 4.7	19.9 ± 4.6	21.8 ± 1.9
	1	55	7	269.9	33.9 ± 4.9	33.9 ± 4.9	20.8 ± 4.1	19.8 ± 2.4	66.3 ± 6.8
CCS	10	25	5	87.6	2.3 ± 0.2	22.6 ± 2.1	11.3 ± 1.8	2.3 ± 0.4	7.4 ± 0.4
	7	25	4	70.1	3.0 ± 0.2	20.7 ± 1.6	9.7 ± 1.4	3.7 ± 0.6	10.4 ± 0.4
	4	25	4	70.1	5.3 ± 0.2	21.3 ± 0.9	10.2 ± 0.7	5.0 ± 0.8	19.7 ± 0.7
XPVP	7	25	5	87.6	3.5 ± 0.2	24.7 ± 1.5	13.1 ± 1.2	1.9 ± 0.3	11.7 ± 0.1
	4	25	5	87.6	6.2 ± 0.0	24.7 ± 0.2	13.1 ± 0.2	2.6 ± 0.2	21.2 ± 0.2
	2	25	4.5	78.9	12.5 ± 0.4	24.9 ± 0.8	13.3 ± 0.7	5.0 ± 0.1	42.6 ± 0.4
	1	25	4	70.1	24.0 ± 0.8	24.0 ± 0.8	12.5 ± 0.7	10.7 ± 1.5	85.3 ± 2.1

Compression length ($L_{c,actual}$) = $t_{phase\ I} \times S$.
Compressibility (C) = (($L_{c,actual}$ − 9)/120)*100 %, where 120 mm is the length of the powder supply unit.
Compression phase ($t_{Phase\ I}$) is average of compression phases of three repeat experiments.
Acceleration phase ($t_{Phase\ II}$) is average of acceleration phases of three repeat experiments.
Stable feeding phase ($t_{Phase\ III}$) is average of stable feeding phases of three repeat experiments.

feeding, the balance cannot reach a stable condition; hence, measurement noise appears in the data recorded at a 1 s interval. A moving mean was introduced to suppress this measurement noise. To ensure the application of a moving mean on the raw data does not eliminate actual feed rate variations, the moving mean method was compared to a time change data analysis method. The time change data analysis method reads the accumulated powder weight (read-out from the balance) at time intervals equal to the moving mean window size. Fig. 5 shows the standard deviations of the time change and moving mean data analysis methods. As the standard deviations of both methods are in good agreement, the application of a moving mean on the raw data does not eliminate actual feed rate variations. The data from both methods demonstrated that a moving mean with a 60 s window is required to suppress the measurement noise. A 60 s moving mean is also accepted in industrial applications (Enabling Technologies Consortium, 2020). Therefore, a 60 s moving mean was applied to all data shown in this study with flow rates greater than 2 g/h. A 120 s window is used when the powder flow rate is under 2 g/h due to the decrease of balance accuracy at low weight measurements.

3.2. Micro-feeding process analysis

The operation of the pneumatic micro-feeder is discussed on the basis of the MCC results (Fig. 3). The results clearly show a degree of similarity to the powder pump performance investigated by (Fathollahi et al., 2020) but without the significant gradual increase of powder flow rate as a function of time.

The feeding process can be broken down into four phases:

1. Phase I - powder compression phase. This system does not require a pre-treatment of the powder. As the powder is freely filled into the powder pump, the powder is compressed by the piston before it is transported upwards towards the entrainment bed. The duration of phase I depends primarily on the compressibility of the powder and the piston speed. This phase can be eliminated by a pre-run, The details of pre-run show in the support information section 3 and Figure S2. It should be noted that the pre-run does not affect the feeding accuracy in Phase III.
2. Phase II - acceleration phase. This phase follows the powder compression phase. The particles are entrained, transferred to the separator, air–solid separated, and then settle to the receiver. The duration of phase II depends on particle size, true density, cohesion, air flow rate, powder feed rate, and separator dimensions.
3. Phase III - stable feeding phase. The system provides consistent powder feeding. Fig. 3 shows a gradual upward slope. It is resulted by the powder compression caused by the wall friction. The powder compression causes two phenomena: 1. The increase of powder bulk density; 2. The excess powder is fed to the entrainment bed. The powder is then slowly accumulated in the entrainment bed and narrowed cross-sectional area. The decrease in the cross-sectional area increases the air velocity, which leads to more particles being picked up. This issue can be minimised by the introduction of automation on adjusting the plug position in future work.
4. Phase IV - shutdown phase. A rapid downward trend occurs as soon as the powder pump stops.

3.3. The influence of equipment configurations and process parameters

3.3.1. Piston speed

The compressibility (C) is defined as the compression degree of the material being compressed in the powder pump due to the wall shear stress. The material compressibility is estimated by considering the dead space of 9 mm in the connection of the powder pump to the chamber of the entrainment bed. The actual compression length of Fig. 3 is 7.4 mm for MCC, yielding a compressibility of 6.2 %. The compressibility is determined by the powder pump diameter, length, powder property and operation. Table 4 summarises phases I and II at different piston speeds. The results indicate that phase I is nearly halved when the piston speed is doubled. The table also shows that the compressibility varies depending on the powder filling.

The lower the feed rate (piston speed) for Phase II, the longer lasts phase II for the same material. This can be attributed to a) the slow particle velocity due to the lower powder flow rate using low air flow rate; b) the fouling in the separator, where particles initially adhere to the separator until the gravity force is greater than the adhesive force. At this point, the system reaches a stable feeding process (phase III). As the fouling rate is nearly constant from our observation, a lower feeding rate at the same equipment setting requires longer to achieve the required fouling quantity. These findings suggest that the duration of phase II is influenced by the powder properties, air flow rate, powder feeding flow rate, and separator dimensions. In addition, phase III gets shorter when the piston speed increases.

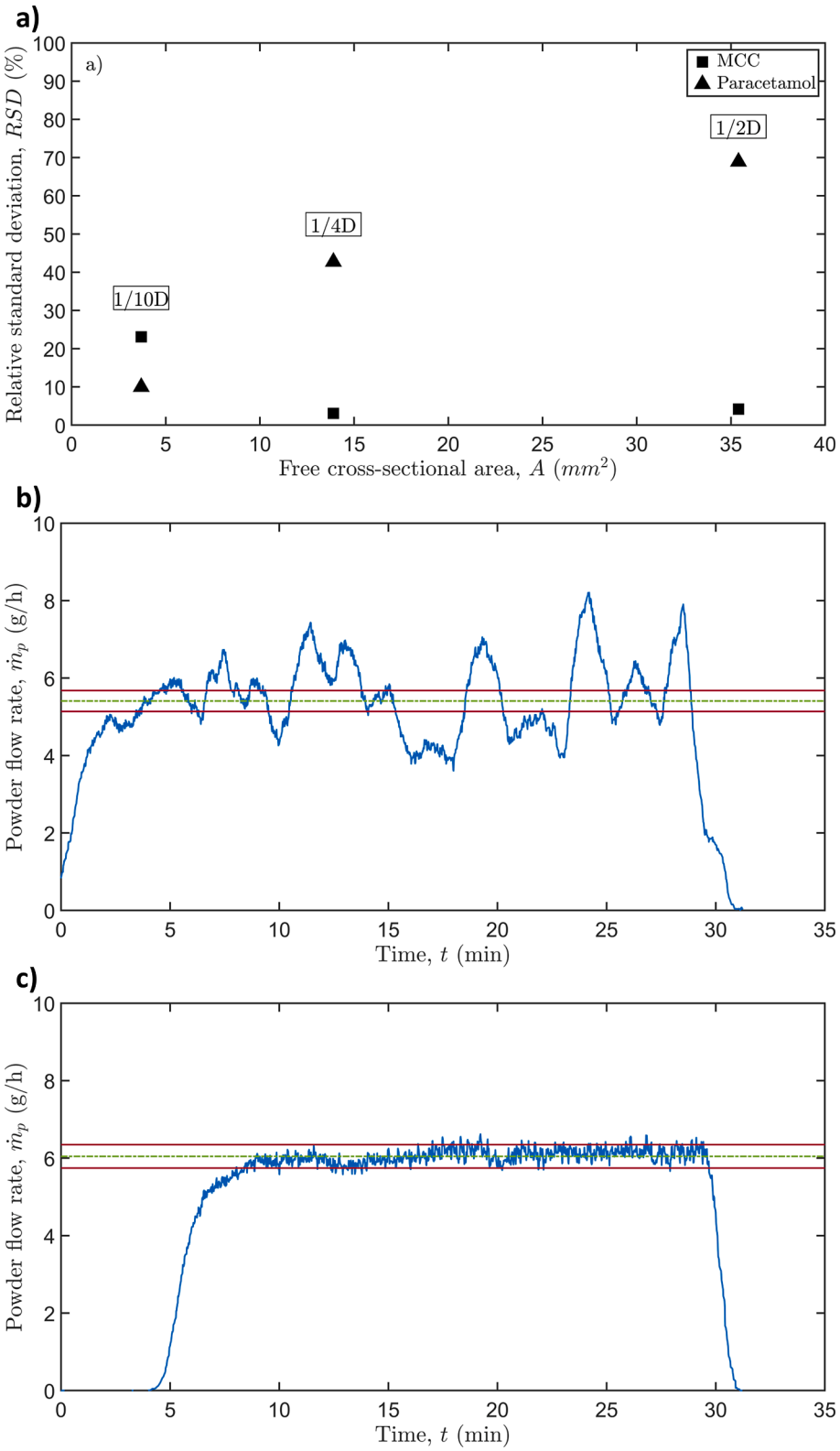

Fig. 6. a) The relative standard deviation of APAP mass flow rate as a function of the cross-section area in the process line controlled by three different insert sizes at a fixed plug position (open position/highest level of the plug). 30 kPa and 9 l/min of air flow rate for the mean powder rate of APAP at 3.4 g/h, 25 kPa of air pressure and 6 l/min of air flow rate for the mean powder rate of MCC at 6.0 g/h; b) the MCC feeding trend using 1/10D cut insert; c) the MCC feeding trend at 1/4D cut insert.

3.3.2. Air supply line and process line inserts

The use of an insert in the air supply line and the process line plays a vital role in controlling powder flow rate stability. The air supply line insert controls the air velocity into the entrainment bed. It prevents back pressure in the air supply line that could cause the powder to settle in the air supply line. The process line insert maintains the air-powder velocity and ensures the particles are suspended in the air. The inserts also minimise the supplied air flow rate, which reduces the workload of the

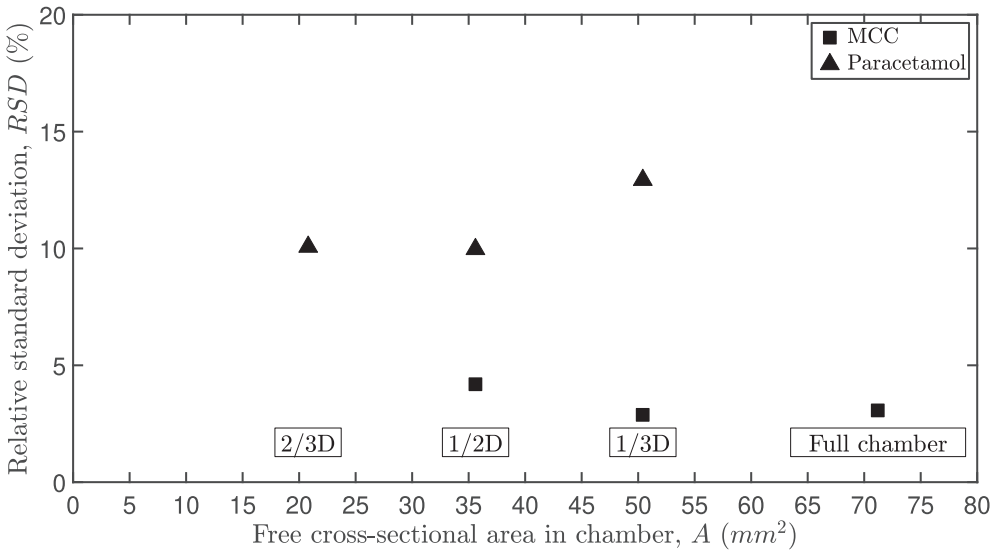

Fig. 7. The relative standard deviation of the MCC flow rate (6 g/h) and APAP flow rate (3.3 g/h) as a function of different plug positions in the entrainment bed using the same insert size (1/10D cut insert for APAP, 1/4D cut insert for MCC) at same air flow rate and pressure settings (30 kPa and 9 l/min of air flow rate for APAP, 25 kPa of air pressure and 6 l/min of air flow rate for MCC).

separator.

Fig. 6 depicts the RSDs of powder flow rates for MCC and APAP as a function of the insert sizes (free cross-section areas). It shows the impact of three different sizes of inserts on the stability of the MCC and APAP powder flow rate. The results demonstrate that an inappropriate insert size causes a higher RSD.

In addition, Fig. 6 demonstrates that the non-flow material (APAP) requires a small insert, whereas the cohesive material (MCC) yields lower RSDs with a large insert. 1/2D insert is required for MCC, whereas 1/10D insert is required for APAP to stabilise the powder flow rate. The kinetic energy of air flow is termed the entrainment energy in this study. As known, the reduction in insert size (free cross-sectional area) increases the air velocity when the air flow rate is constant. It dramatically raises the air flow kinetic energy based on the kinetic energy equation of air flow. Without the insert, a higher air flow rate would be required to achieve the desired air velocity, adding excess entrained energy to the system and causing fluctuations. It would also require a wide range of air flow rate meter and controller to achieve the ideal air velocity. Therefore, the appropriate insert size selection for individual materials helps to maximise entrainment efficiency and entrainment rate.

3.3.3. *Plug position*

Adjustment of the plug position regulates the air velocity and pressure drop in the entrainment chamber. This study investigated the influence of four discrete positions (full open chamber, 1/3D, 1/2D and 2/3D) on the stability of the powder flow rate. Fig. 7 illustrates the RSDs of MCC and APAP powder flow rate as a function of three different plug positions using the same insert size. It suggests that a 1/10D cut insert with the plug position at 1/2D provides stable feeding for APAP, and the use of a 1/4D cut insert with the plug position at 1/3D results in stable feeding for MCC. It was found that placing the plug below the optimal position will increase the air velocity and entrainment energy and cause strong turbulence in the chamber. This turbulence will dig out powder from the powder feed unit, entrain excess powder to the outlet, and cause fluctuations in the powder flow rate. On the contrary, when the position of the plug is higher than the optimal position, the low air

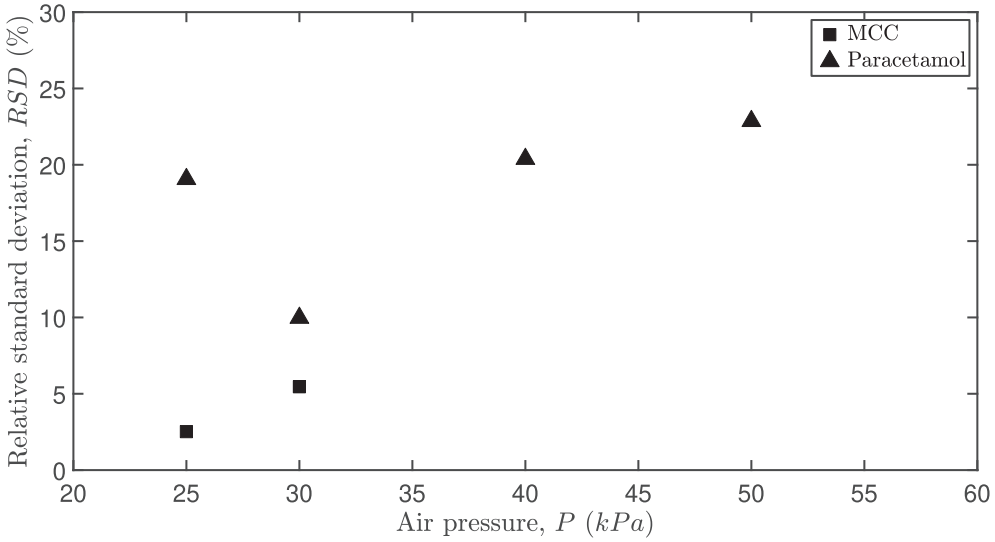

Fig. 8. The relative standard deviation of the APAP flow rate (3.5 g/h) and MCC flow rate (6 g/h) as a function of the air pressure at 9 l/min of air low rate. A plug position of 1/2D and an insert size of 1/10D cut was set for APAP, and a plug position of 1D and an insert size of 1/2D cut for MCC.

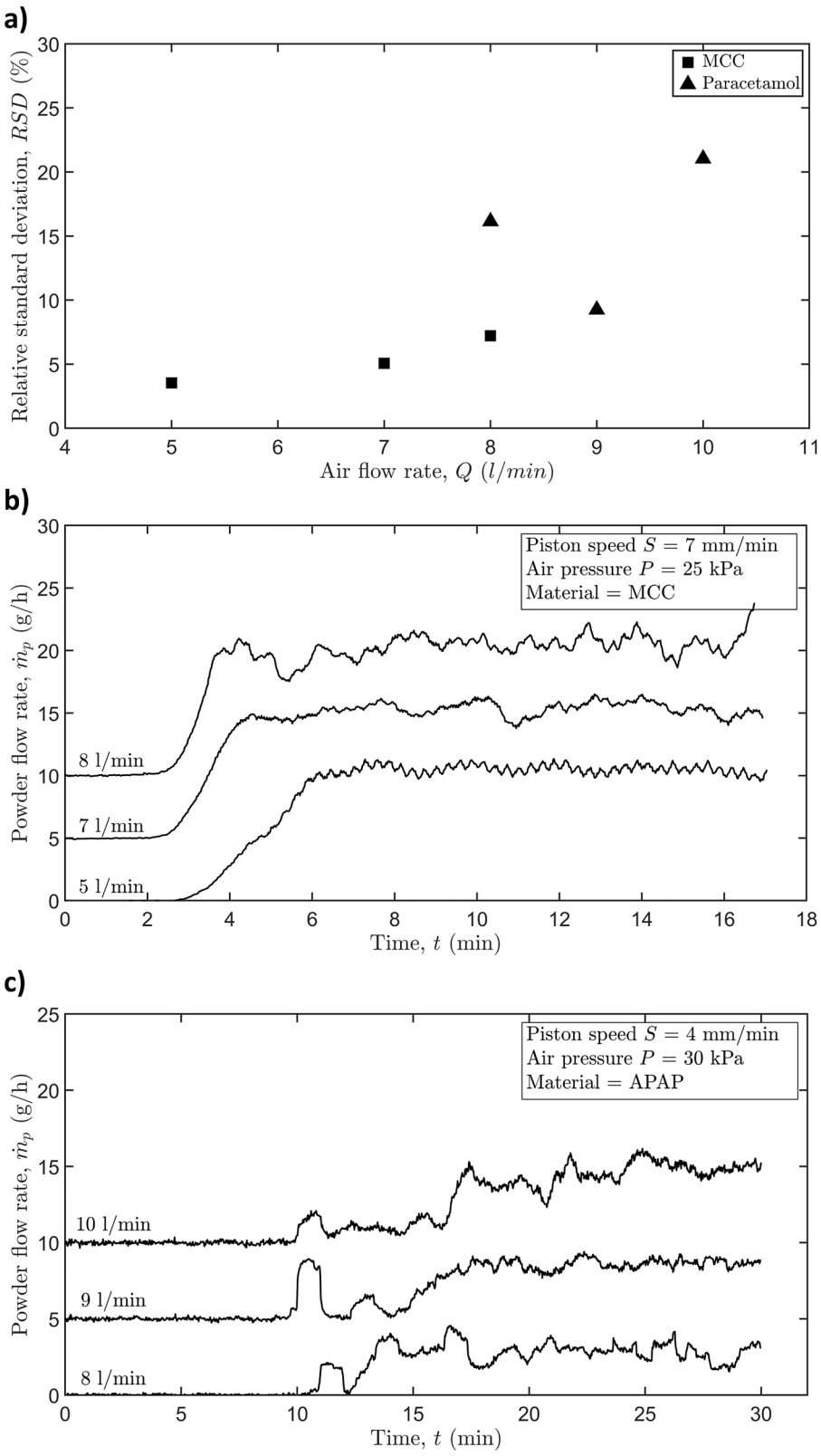

Fig. 9. Feeding performance of MCC and APAP for different setting. a) The effect of air flow rate on the MCC flow rate (6 g/h) and APAP flow rate (3.5 g/h) at a fixed piston speed and equipment setting. It shows the RSDs of MCC (■) and APAP (▲) powder flow rate as a function of the air flow rate at fixed air pressures (25 kPa and 30 kPa) and plug positions (full chamber and 1/2D) with the same insert size (1/2D cut and 1/10D cut); b) the effect of air flow rate on the MCC powder flow rate; c) the effect of air flow rate on the APAP powder flow rate.

velocity (low entrainment energy) will result in poor entrainment efficiency, which in turn causes the system to be blocked by the accumulation of powder in the chamber. Therefore, the selection of plug position together with the insert size are critical settings in terms of the stability of the powder flow rate.

3.3.4. Air pressure

The air pressure affects the chamber's air velocity and air flow rate influencing the entrainment energy. Fig. 8 shows the RSDs of APAP and MCC powder flow rate as a function of air pressure at 9 l/min of air low rate. A plug position of 1/2D and an insert size of 1/10D cut were set for APAP feeding, and a plug position of the full chamber and an insert size

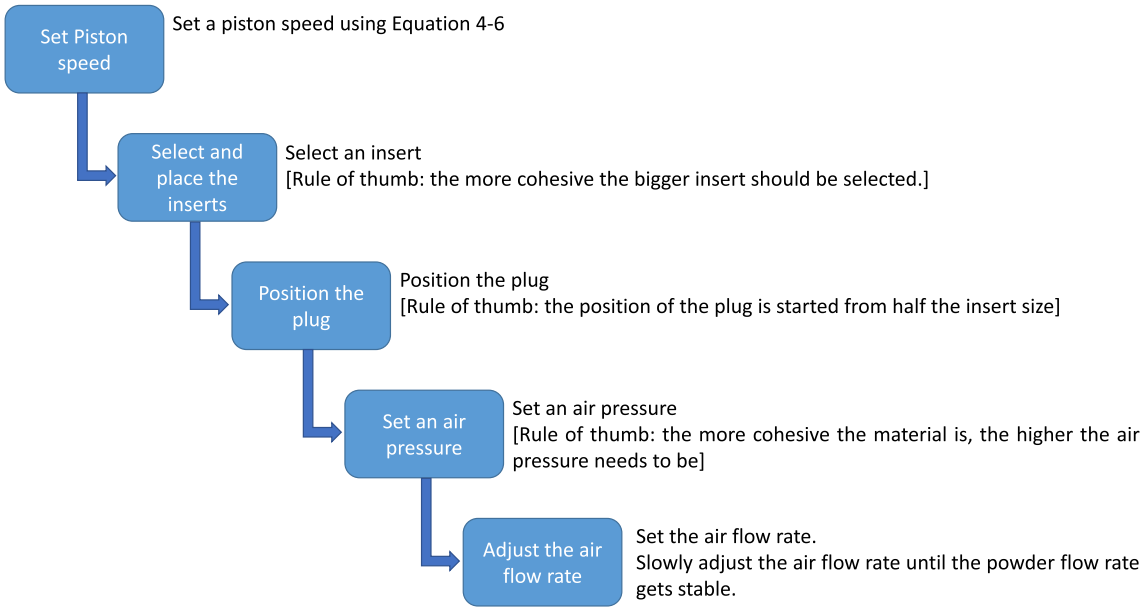

Fig. 10. The equipment and operational guideline.

of 1/2D cut were set for MCC feeding. The figure indicates that the optimal air pressure point should be around 30 kPa for APAP and 25 kPa for MCC, where lower or higher air pressure leads to severe fluctuations.

3.3.5. *Air flow rate*

The air flow rate is used to minimise the variations of the powder flow rate. Fig. 9 clearly show that the variations were minimised by reducing the air flow rate, and a stable MCC powder feeding rate was achieved using an air flow rate of 5 l/min. It is found that the RSDs increase with raising the air flow rate for MCC. The powder flow rate can be stabilised through air entrainment, which can also be clearly observed for APAP feeding.

Fig. 9 shows that three phenomena occur when the air flow rate is not close to the optimal value: First, when the air flow rate is higher, the air acts as a scraper. Due to the compression in the powder pump, the powder density is reduced across the displacement. Therefore, the powder flow rate tends to increase gradually. The obtained metrics from this scenario would be similar to the powder pump's original design (Besenhard et al., 2017; Fathollahi et al., 2020). Second, fluctuations occur for air flow rates higher than the optimal value due to large agglomerates entrained, especially for cohesive materials. Third, blockage occurs when the air flow rate is lower than optimal. This is because powder feeding from the powder pump to the entrainment bed is faster than the powder flow entrained by the air, which leads to accumulation in the chamber. According to these findings, the exact ratio between piston speed and air flow rate is vital for stabilising the powder flow rate.

3.3.6. *Equipment and operational guideline*

Based on the influence of equipment configurations and process parameters, a recommendation can be made for equipment and operational settings. The equipment settings and process parameters can be determined and broken down into four steps to find the optimal equipment setting and process parameters. These stages can be defined as follows:

Step 1 - Set the piston speed.

In order to predict the piston speed setting, the piston speed (S) and

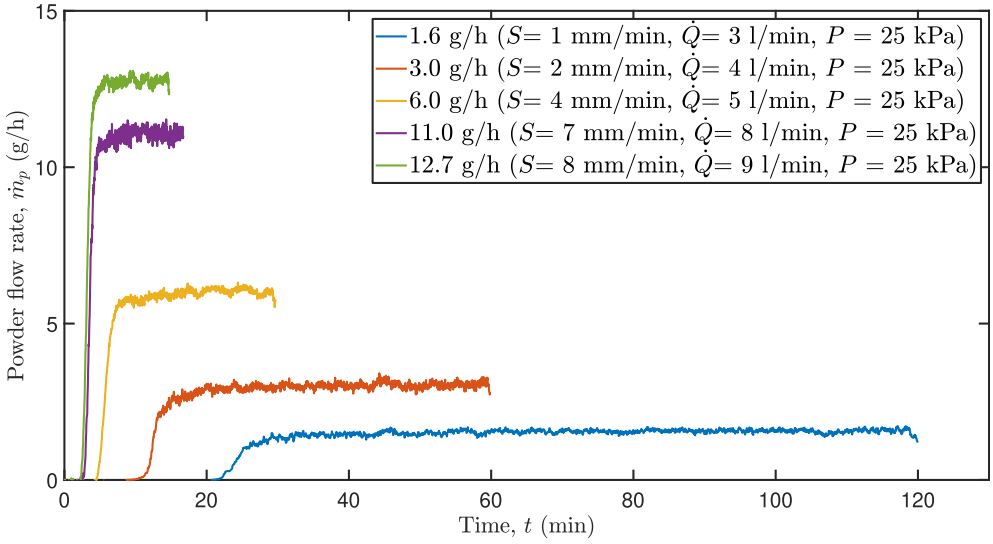

Fig. 11. Feeding performance of MCC using the pneumatic micro-feeder. The air pressure, P, was set at 25 kPa. The air flow rate, $\dot{Q}$, was adjusted to stabilise the powder flow rate. The piston speed, S, was varied to adjust the average powder flow rate.

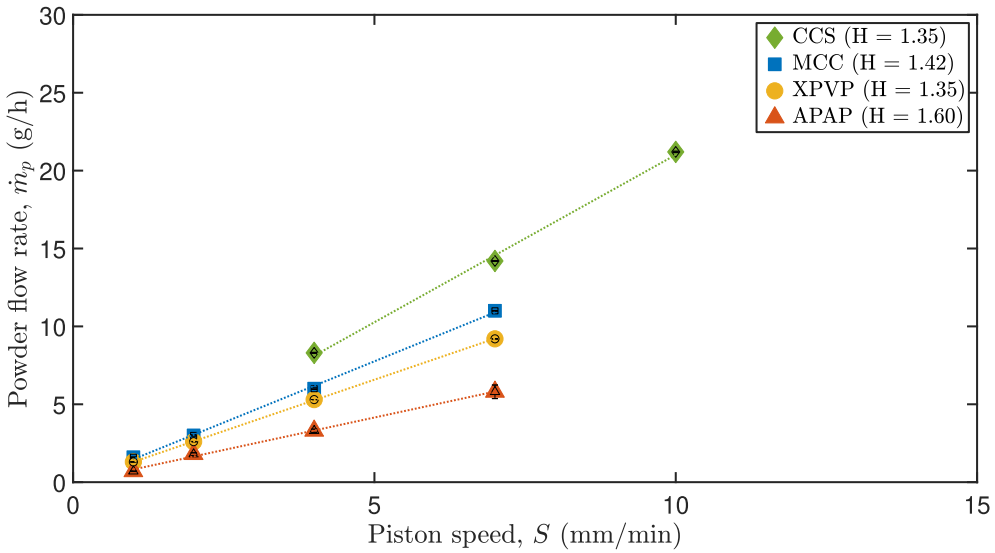

Fig. 12. Average powder mass flow rate with standard deviations of three repeat experiments as a function of piston speed for four different materials. *H* represents Hausner ratio.

the mean powder feed rate ($\dot{m}_{p,b}$) was estimated following

$$\mathrm{m_{p.b}} = S\rho_{\mathrm{b}}A_{\mathrm{b}}/(1-C) \tag{8}$$

where ρ_{b} is the powder bulk density, A_{b} is the cross-section area of the powder pump. In this study, A_{b} is 71.18 mm^2. C is the powder compression. The full derivation steps can be found in the support information section 4. Equation (8) helps estimate the piston speed setting when the desired powder flow rate is known. In this study, the current motor can only set integer values. In future work, a wider range of motor speed settings will provide a more accurate powder flow rate.

Step 2 - Select insert.

We know from section 3.3.2 that non-flow materials (APAP) require a small free cross-sectional area insert. In contrast, the cohesive material (MCC) requires a large free cross-sectional area insert. Therefore, a suitable inset size requires several tests and needs to consider the flowability of the material.

Step 3 - Position of the plug.

The plug's positioning starts from half of the insert size, e.g. the plug would be positioned at 1/3D for a selected 1/4D cut insert and is then increased or decreased until the optimal plug position is found.

Step 4 - Set air pressure and air flow rate.

Using MCC as a baseline, MCC used 25 kPa of air pressure in this study. For cohesive material, high entrainment energy is expected, which can be achieved by increasing the air velocity or air mass flow rate. To increase the air velocity, it is by adjusting the air pressure and air flow rate. The higher air pressure would also be considered to increase the air mass flow rate. For example, we know that APAP has a higher cohesion force between particles than MCC. Therefore, 30 kPa of air pressure was selected in APAP feeding experiments. The air flow rate is then slightly adjusted to minimise the RSDs. As a rule of thumb, the more cohesive the material, the higher the air pressure and air flow rate should be. In addition, the air flow rate should be increased when powder accumulation is observed in the process line. When the powder flow rate is seen to fluctuate, the air flow rate should be reduced. Fig. 10 summarises the equipment and operational guideline.

3.4. Feeding performance of different materials

Fig. 11 shows the feeding performance of MCC for five powder flow rates between 1.6 g/h and 12.7 g/h. It clearly demonstrates a consistent feeding and a positive correlation between the piston speed and powder flow rate. Further analysis showed that the air flow rate adjustment minimises the RSDs to below ± 5 %. The system can consistently feed for 80 min for the lowest MCC feeding performance (1.6 g/h).

Fig. 12 summarises the average powder flow rate for four materials as a function of piston speed. As expected, the powder flow rate increases linearly with increasing piston speed. However, the currently available data does not provide sufficient information to confirm the relationship of the slopes to cohesion, particle size or bulk density.

Table 5 summarises the overall feeding performance of the four materials. Across all materials, the pneumatic micro-feeder demonstrated high repeatability and can consistently feed powders within the range of 0.7 g/h to 21.2 g/h with an RSD of less than ± 5–20 % (depending on the material).

In the case of cohesive powder (MCC), the micro-feeder was able to achieve feed rates ranging from 1.6 ± 0.07 g/h to 11 ± 0.22 g/h with RSDs of < ±5%, high repeatability (<1.5 %) and high stability (<0.5 %). For the non-flow material APAP, the current equipment setting can feed APAP from 0.7 g/h (< ±20 %) to 5.8 g/h (< ±10 %) with repeatability of < 8 % and stability of < 5 %. Applied to a powder with a low Hausner ratio of 1.35, the micro-feeder was able to feed CCS from 8.3 g/h to 21.2 g/h with an RSD < 16 %, repeatability of < 5 % and stability of < 1.5 %. And it was shown to be capable of feeding XPVP at a feed rate from 9.2 g/h ± 5 % to 1.3 g/h ± 10 % with a repeatability of<1.5 % and better than 1.3 % stability. Although CCS and XPVP have a similar Hausner ratio ($H = 1.35$), CCS increased the RSD at a low powder flow rate. Conversely, the feeder performance for XPVP was significantly better. Comparing the particle size of both materials, XPVP ($D_{50} = 104.9$ μm) particles are on average twice as large as CCS particles ($D_{50} = 54.9$ μm). These results indicate that the particle size also affects the feeding consistency.

According to Table 3, APAP with a Hausner ratio greater than 1.60 is classified as a non-flowing material. APAP, therefore, represents a challenging material to assess the capabilities of this design. Fig. 13 compares the feeding performance of APAP and MCC at similar powder flow rates. APAP requires a higher piston speed (7 mm/min) to achieve the same powder flow rate as MCC (4 mm/min). This is due to the higher compressibility of APAP (Table 4); APAP is twice as compressible as MCC. Phase I of APAP is thus longer than that of MCC. Additionally, the acceleration phase of APAP is 6.9 min compared to 4.8 min of MCC, which is primarily attributed to the higher cohesive forces of APAP. APAP also adheres more strongly to the inner wall of the separator, which leads to an extended phase II. APAP particle size is smaller than MCC's, extending the particle settling time. Due to the extension of

Table 5
Summary of the feeding performance of different powder flow rates. The definitions of all listed parameters can be found in section 3.2.

Materials	Piston speed, S (mm/min)	Air pressure, P (kPa)	Air flow rate, Q (l/min)	Air mass flow rate, $\dot{m}_{air}$ (g/h)	Powder flow rate, $\dot{m}_p$ (g/h)	Standard deviation, σ (g/h)	Relative standard deviation, RSD (%)	Average powder flow rate, $\bar{\dot{m}}_p$ (g/h)	Average standard deviation, $\bar{\sigma}$ (g/h)	Average relative standard deviation, $\bar{R}\bar{S}\bar{D}$ (%)	Repeatability, r (%)	Stability, s (%)
Microcrystalline cellulose (MCC)	7	25	8	140.2	11.0	0.2151	2.0	11.0	0.2191	2.0	0.20	0.13
					11.0	0.2068	1.9					
					11.0	0.2354	2.1					
	4	25	5	87.6	5.9	0.1740	2.9	6.0	0.1699	2.9	0.78	0.12
					5.9	0.1615	2.7					
					6.0	0.1742	2.9					
	2	25	4	70.1	3.0	0.1049	3.5	3.0	0.1152	3.8	1.31	0.44
					3.0	0.1291	4.3					
					3.1	0.1116	3.6					
	1	25	3	52.6	1.6	0.0680	4.3	1.6	0.0716	4.5	0.55	0.39
					1.6	0.0682	4.3					
					1.6	0.0787	5.0					
Paracetamol (APAP)	7	50	10	350.5	6.2	0.3670	5.9	5.8	0.3645	6.4	7.56	1.15
					5.7	0.3154	5.5					
					5.4	0.4112	7.7					
	4	30	9	189.3	3.4	0.3913	11.6	3.3	0.3631	10.6	3.05	0.86
					3.6	0.3548	10.0					
					3.4	0.3433	10.2					
	2	25	9	157.7	1.7	0.1732	10.0	1.8	0.1612	9.0	4.80	1.17
					1.8	0.1353	7.7					
					1.9	0.1752	9.3					
	1	55	7	269.9	0.7	0.0964	13.6	0.7	0.1317	19.2	2.72	4.93
					0.7	0.1421	21.1					
					0.7	0.1567	22.9					
Croscarmellose sodium (CCS)	10	25	5	87.6	20.2	1.7250	8.5	21.2	1.7889	8.4	4.32	0.50
					21.4	1.6867	7.9					
					22.1	1.9550	8.9					
	7	25	4	70.1	13.9	1.8041	13.0	14.2	1.6779	11.8	2.46	1.29
					14.1	1.7086	12.1					
					14.6	1.5210	10.4					
	4	25	4	70.1	8.6	1.5276	17.7	8.3	1.3488	16.2	3.14	1.52
					8.1	1.1958	14.7					
					8.2	1.3232	16.1					
Crospovidone (XPVP)	7	25	5	87.6	9.1	0.2800	3.1	9.2	0.3286	3.6	0.97	0.45
					9.2	0.3414	3.7					
					9.2	0.3643	4.0					
	4	25	5	87.6	5.3	0.2493	4.7	5.3	0.2312	4.3	0.54	0.34
					5.3	0.2128	4.0					
					5.4	0.2317	4.3					
	2	25	4.5	78.9	2.7	0.1910	7.2	2.6	0.2238	8.5	1.32	1.22
					2.6	0.2472	9.5					
					2.6	0.2332	8.9					
	1	25	4	70.1	1.3	0.1312	9.9	1.3	0.1241	9.5	0.72	0.43
					1.3	0.1225	9.4					
					1.3	0.1185	9.1					

Powder flow rate: the average of each calculated powder flow rate after the flow rate stabilised (Phase III)
Average powder flow rate: the average of powder flow rate of three repeat experiments
Standard deviation (SD): the average of standard deviation after the flow rate stabilised (Phase III)
Average SD: the average of standard deviations of three repeat experiments
Relative Standard Deviation (RSD) = SD/powder flow rate
Average RSD: the average of RSD of three repeat experiments
Repeatability = standard deviation of powder flow rates/average powder flow rate
Stability = standard deviation of RSDs of three repeat experiments

phases I and II, the stable phase of APAP becomes shorter compared to the stable phase of MCC. Table 5 shows that the air mass flow rate of APAP is almost twice of that of MCC. This finding, while preliminary, suggests that a higher air entrainment rate is required to overcome cohesion. Further work should be undertaken to investigate the relationship between the air entrainment rate and cohesion.

3.5. Current limitations of the pneumatic micro-feeder

However, its current limitations can be summarised as follows (the details of limitation and disturbance can be found in the support information section 5 and 6 and Figures S3 – S7):

- Fouling in the separator, especially for materials with a particle size < 50 μm (see Table S2 in supporting information); further research will investigate the effectiveness of minimising the fouling using an ultrasonic vibrator.
- Segregation of non-flow materials such as APAP; like the first point (fouling in the separator), the application of ultrasonic vibration is expected to minimise segregation.
- Relatively short stable feed time; further research will introduce a continuous powder feeding unit to replace the limitation of the powder pump.

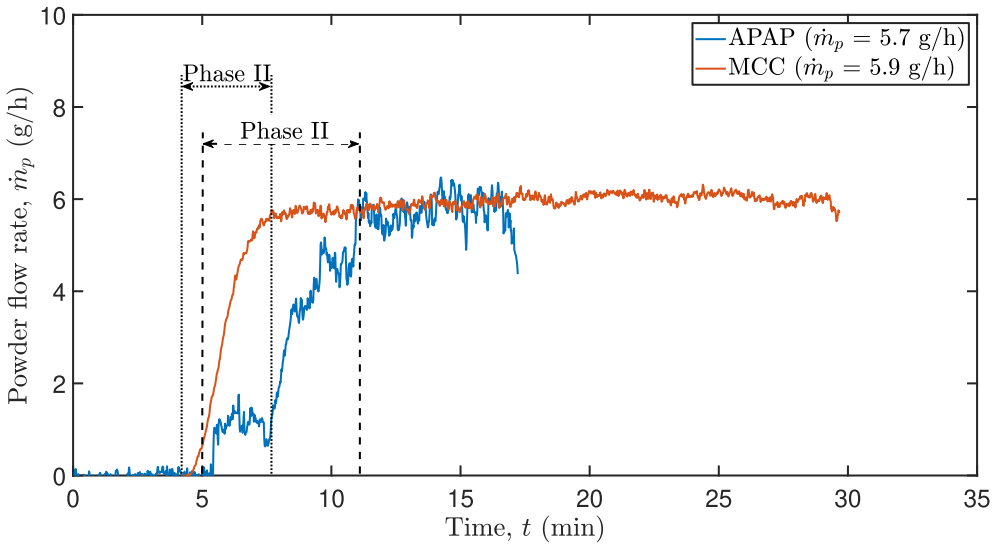

Fig. 13. Comparison of MCC and APAP at similar feed rates. The parameters of MCC were set to 4 mm/min of piston speed, 25 kPa of air pressure and 5 l/min of air flow rate. APAP was fed at 7 mm/min of piston speed, 50 kPa of air pressure and 10 l/min of air flow rate.

4. Conclusions

A novel pneumatic micro-feeder was developed, and its performance was demonstrated for four different pharmaceutical-grade materials. This system shows its potential for delivering consistent powder flow rate controlled by adjusting the air flow rate. This system has only a few moving parts, is composed of simple components, and is easy to operate. The effects of process parameters and equipment configurations on feed performance, including different insert sizes, plug positions, air pressure, air flow rate, and piston speed were investigated. The overall results show that this system can feed a powder flow rate of 0.7 to 20 g/h, with an RSD of ± 20 to 5 %, depending on the powder properties. The feeder demonstrates a high degree of repeatability and stability. The results of this work can be summarised as follows:

- The powdery material does not need to be pre-conditioned.
- The powder flow rate has no significant increase of powder flow rate over time as the powder pump has.
- The system can consistently feed powder down to 0.7 g/h of powder flow rate.
- The system can handle a wide range of powder properties.
- The system provides good repeatability and stability of low-quantity powder feeding.
- The system shows its controllability of a constant flow rate for a range of powder flow rates by adjusting the piston speed and air flow rate.
- This system does not require high air pressure and flow rate, and the air can be replaced by another gas, such as nitrogen, for various purposes.

In conclusion, this system's high consistency and low dose/flow rate will be particularly beneficial for manufacturing future solid oral dosage forms, such as HPAPI products. Future work will develop a continuous powder micro-feeder and introduce automation into the system to improve its accuracy and to meet current good manufacturing practice (cGMP) industrial applications.

CRediT authorship contribution statement

P. Hou: Conceptualization, Investigation, Formal analysis, Methodology, Visualization, Writing – original draft. **M.O. Besenhard:** Supervision, Writing – review & editing, Funding acquisition. **G. Halbert:** Supervision, Writing – review & editing. **M. Naftaly:** Supervision, Writing – review & editing, Funding acquisition. **D. Markl:** Supervision, Conceptualization, Writing – review & editing, Project administration, Funding acquisition.

Declaration of Competing Interest

The authors declare that they have no known competing financial interests or personal relationships that could have appeared to influence the work reported in this paper.

Data availability

Data will be made available on request.

Acknowledgements

The authors would like to thank the University of Strathclyde, the Centre for Continuous Manufacturing and Advanced Crystallisation and the National Physical Laboratory for funding this work. The authors would like to acknowledge that this work was carried out in the CMAC National Facility supported by UKRPIF (UK Research Partnership Fund) award from the Higher Education Funding Council for England (HEFCE) (Grant ref HH13054).

Appendix A. Supplementary data

Supplementary data to this article can be found online at https://doi.org/10.1016/j.ijpharm.2023.122691.

References

Annamalai, K., Ruiz, M., Vo, N., Anand, V., 1992. Locally fluidizing feeder for powder transport. Powder Technology 73, 181–190. https://doi.org/10.1016/0032-5910(92)80079-C.

Barati Dalenjan, M., Jamshidi, E., Ale Ebrahim, H., 2015. A screw-brush feeding system for uniform fine zinc oxide powder feeding and obtaining a homogeneous gas-particle flow. Advanced Powder Technology 26, 303–308. https://doi.org/10.1016/j.apt.2014.10.010.

Besenhard, M.O., Faulhammer, E., Fathollahi, S., Reif, G., Calzolari, V., Biserni, S., Ferrari, A., Lawrence, S.M., Llusa, M., Khinast, J.G., 2015. Accuracy of micro powder dosing via a vibratory sieve – chute system. European Journal of Pharmaceutics and Biopharmaceutics 94, 264–272. https://doi.org/10.1016/j.ejpb.2015.04.037.

Besenhard, M.O., Karkala, S.K., Faulhammer, E., Fathollahi, S., Ramachandran, R., Khinast, J.G., 2016. Continuous feeding of low-dose APIs via periodic micro dosing.

International Journal of Pharmaceutics 509, 123–134. https://doi.org/10.1016/j.ijpharm.2016.05.033.
Besenhard, M.O., Fathollahi, S., Siegmann, E., Slama, E., Faulhammer, E., Khinast, J.G., 2017. Micro-feeding and dosing of powders via a small-scale powder pump. International Journal of Pharmaceutics 519, 314–322. https://doi.org/10.1016/j.ijpharm.2016.12.029.
Blackshields, C.A., Crean, A.M., 2018. Continuous powder feeding for pharmaceutical solid dosage form manufacture: a short review. Pharm Dev Technol 23, 554–560. https://doi.org/10.1080/10837450.2017.1339197.
Bostijn, N., Dhondt, J., Ryckaert, A., Szabó, E., Dhondt, W., Van Snick, B., Vanhoorne, V., Vervaet, C., De Beer, T., 2019. A multivariate approach to predict the volumetric and gravimetric feeding behavior of a low feed rate feeder based on raw material properties. International Journal of Pharmaceutics 557, 342–353. https://doi.org/10.1016/j.ijpharm.2018.12.066.
Burcham, C.L., Florence, A.J., Johnson, M.D., 2018. Continuous Manufacturing in Pharmaceutical Process Development and Manufacturing. Annual Review of Chemical and Biomolecular Engineering 9, 253–281. https://doi.org/10.1146/annurev-chembioeng-060817-084355.
Enabling Technologies Consortium, 2020. POWDER FEEDING SYSTEM [WWW Document]. etconsortium.org. URL https://www.etconsortium.org/powderfeedingsystem.
Engisch, W.E., Muzzio, F.J., 2014. Loss-in-Weight Feeding Trials Case Study: Pharmaceutical Formulation. Journal of Pharmaceutical Innovation 10, 56–75. https://doi.org/10.1007/s12247-014-9206-1.
Engisch, W.E., Muzzio, F.J., 2015. Feedrate deviations caused by hopper refill of loss-in-weight feeders. Powder Technology 283, 389–400. https://doi.org/10.1016/j.powtec.2015.06.001.
Fathollahi, S., Sacher, S., Escotet-Espinoza, M.S., Dinunzio, J., Khinast, J.G., 2020. Performance Evaluation of a High-Precision Low-Dose Powder Feeder. AAPS PharmSciTech 21. https://doi.org/10.1208/s12249-020-01835-5.
Fathollahi, S., Kruisz, J., Sacher, S., Rehrl, J., Escotet-Espinoza, M.S., DiNunzio, J., Glasser, B.J., Khinast, J.G., 2021. Development of a Controlled Continuous Low-Dose Feeding Process. AAPS PharmSciTech 22, 1–14. https://doi.org/10.1208/s12249-021-02104-9.
Francis, T.M., Kreider, P.B., Lichty, P.R., Weimer, A.W., 2010. An investigation of a fluidized bed solids feeder for an aerosol flow reactor. Powder Technology 199, 70–76. https://doi.org/10.1016/j.powtec.2009.04.020.
Hartman, M., Phořelý, M., Trnka, O., 2006. Transport velocities of different particulate materials in pneumatic conveying. Chemical Papers- Slovak Academy of Sciences 60, 74–77. https://doi.org/10.2478/s11696-006-0015-y.
Jamróz, W., Szafraniec, J., Kurek, M., Jachowicz, R., 2018. 3D Printing in Pharmaceutical and Medical Applications – Recent Achievements and Challenges. Pharmaceutical Research 35. https://doi.org/10.1007/s11095-018-2454-x.
Jassim-Jaboori, A.H., Oyewumi, M.O., 2015. 3D Printing Technology in Pharmaceutical Drug Delivery: Prospects and Challenges. Journal of Biomolecular Research & Therapeutics 4, e141. https://doi.org/10.4172/2167-7956.1000e141.
Kousaka, Y., Okuyama, K., Endo, Y., 1980. Re-entrainment of small aggregate particles from a plane surface by air stream. JOURNAL OF CHEMICAL ENGINEERING OF JAPAN 13, 143–147. https://doi.org/10.1252/jcej.13.143.
Matsusaka, S., Masuda, H., 1996. Particle Reentrainment from a Fine Powder Layer in a Turbulent Air Flow. Aerosol Science and Technology 6826, 69–84. https://doi.org/10.1080/02786829608965353.
McGlinchey, D., 2009. Bulk Solids Handling: Equipment Selection and Operation, Bulk Solids Handling: Equipment Selection and Operation. 10.1002/9781444305449.
Nagy, Z.K., Hagrasy, A. El, Litster, J., 2020. Book of Continuous Pharmaceutical Processing.
Oladeji, S., Mohylyuk, V., Jones, D.S., Andrews, G.P., 2022. 3D printing of pharmaceutical oral solid dosage forms by fused deposition: The enhancement of printability using plasticised HPMCAS. International Journal of Pharmaceutics 616, 121553. https://doi.org/10.1016/j.ijpharm.2022.121553.
Quodbach, J., Bogdahn, M., Breitkreutz, J., Chamberlain, R., Eggenreich, K., Elia, A.G., Gottschalk, N., Gunkel-Grabole, G., Hoffmann, L., Kapote, D., Kipping, T., Klinken, S., Loose, F., Marquetant, T., Windolf, H., Geißler, S., Spitz, T., 2021. Quality of FDM 3D Printed Medicines for Pediatrics: Considerations for Formulation Development, Filament Extrusion, Printing Process and Printer Design. Therapeutic Innovation and Regulatory Science. 10.1007/s43441-021-00354-0.
Raijada, D., Wac, K., Greisen, E., Rantanen, J., Genina, N., 2021. Integration of personalized drug delivery systems into digital health. Advanced Drug Delivery Reviews, 113857. https://doi.org/10.1016/j.addr.2021.113857.
Ramachandran, V., Halfpenny, P.J., Roberts, K.J., 2017. Crystal science fundamentals, NATO Science for Peace and Security Series A: Chemistry and Biology. 10.1007/978-94-024-1117-1_1.
Schulze, D., Schwedes, J., Carson, J.W., 2008. Powders and bulk solids: Behavior, characterization, storage and flow. Powders and Bulk Solids: Behavior, Characterization, Storage and Flow 1–511. https://doi.org/10.1007/978-3-540-73768-1.
Stranzinger, S., 2018. Novel stand-alone test tool for scientific qualification of a dosator capsule filling process.
Suri, A., Horio, M., 2009. A novel cartridge type powder feeder. Powder Technology 189, 497–507. https://doi.org/10.1016/j.powtec.2008.08.001.
Theerachaisupakij, W., Matsusaka, S., Akashi, Y., Masuda, H., 2003. Reentrainment of deposited particles by drag and aerosol collision. Journal of Aerosol Science 34, 261–274. https://doi.org/10.1016/s0021-8502(02)00180-5.
Wang, H., Wu, L., Zhang, T., Chen, R., Zhang, L., 2018a. Continuous micro-feeding of fine cohesive powders actuated by pulse inertia force and acoustic radiation force in ultrasonic standing wave field. International Journal of Pharmaceutics 545, 153–162. https://doi.org/10.1016/j.ijpharm.2018.05.006.
Wang, H., Zhang, T., Zhao, M., Chen, R., Wu, L., 2018b. Micro-dosing of fine cohesive powders actuated by pulse inertia force. Micromachines 9. https://doi.org/10.3390/mi9020073.